Progressive Acylation of Pyrene Engineers Solid State Packing and Colour via C–H···H–C, C–H···O and π–π Interactions

*Shinaj K. Rajagopal, Abbey M. Philip, Kalaivanan Nagarajan and Mahesh Hariharan**

School of Chemistry, Indian Institute of Science Education and Research Thiruvananthapuram, CET Campus,
Sreekaryam, Thiruvananthapuram, Kerala, INDIA 695016

E-mail: mahesh@iisertvm.ac.in or mahesh.hrn@gmail.com

Supplementary Information

	1AP and **2”AP)** and 550 nm (for **2AP**, **2’AP**, **3AP** and **4AP)**.	
21	**Fig. S12** Shows the normalised (a) absorption and (b) fluorescence emission spectra of crystalline **1-4AP** derivatives; excitation wavelength is 350 nm and (c) fluorescence decay profile of crystalline **2-4AP** derivatives and the corresponding inset shows fluorescence decay profile of crystalline **1AP**, excitation wavelength is 375 nm and emission monitored at 518 nm (**1AP**); 602 nm (**2AP**); 567 nm (**2’AP**); 631 nm(**2”AP**); 645 nm (**3AP**) and 646 nm (**4AP**).	19
22	**Fig. S13** Shows CIE colour diagram of fluorescence emission for crystalline **1-4AP** derivatives.	19
23	**Fig. S14** Shows fluorescence excitation spectra of crystalline a) **1AP**; b) **2AP**; c) **2’AP**; d) **2”AP**; e) **3AP** and f) **4AP** as compared to absorption spectra. Absorption spectra of crystalline **1-4AP** derivative are reproduced from **Fig. S12a** for comparison with excitation spectra. Emission maxima, where the excitation spectra are monitored, are indicated in the bracket.	20

Materials and methods

All chemicals were obtained from commercial suppliers and used as received without further purification. All reactions were carried out in oven-dried glassware prior to use and wherever necessary, were performed under dry nitrogen in dried, anhydrous solvents using standard gastight syringes, cannulae, and septa. Solvents were dried and distilled by standard procedures. TLC analysis were performed on precoated aluminum plates of silica gel 60 F254 plates (0.25 mm, Merck) and developed TLC plates were visualized under short and long wavelength UV lamps. Flash column chromatography was performed using silica gel of 200-400 mesh employing a solvent polarity correlated with the TLC mobility observed for the substance of interest. Yields refer to chromatographically and spectroscopically homogenous substances. Melting points were obtained using a capillary melting point apparatus and are uncorrected. IR spectra were recorded on a Shimadzu IRPrestige-21 FT-IR spectrometer as KBr pellets. ^{1}H and ^{13}C NMR spectra were measured on a 500 MHz Bruker advanced DPX spectrometer. Internal standard used for ^{1}H and ^{13}C NMR is 1,1,1,1-tetramethyl silane (TMS). All the elemental analyses were performed on Elementar Vario MICRO Cube analyzer. All values recorded in elemental analyses are given in percentages. Reference standard used for elemental analysis is 4-aminobenzenesulphonic acid (sulphanilic acid).

Thermal Analysis: Differential scanning calorimetric (DSC) analyses were performed in TA DSC Q20. The experiments were done under nitrogen atmosphere, by applying a heating ramp from 25 to 300 °C with a heating rate of 10 °C/min. The integral under the DSC peak, above the baseline, gives the total enthalpy change for the melting process.

$$\int \left\{\frac{dH}{dt}\right\}_{sample} dt = \Delta \mathrm{H}_{sample} \quad (1)$$

Spectral Measurements: Absorption spectra were recorded on Shimadzu UV-3600 UV-VIS-NIR while fluorescence and excitation spectra were performed on Horiba Jobin Yvon Fluorolog spectrometers respectively. The excitation wavelength used is 350 nm unless otherwise mentioned. Fluorescence lifetime measurements were carried out in an IBH picosecond single photon counting system. The fluorescence decay profiles were de-convoluted using IBH data station software version 2.1, and fitted with exponential decay, minimizing the $\chi 2$ values of the fit to 1 ± 0.05. All spectroscopic experiments were performed by using standard quartz cuvettes of path length 1cm for solution in dried and distilled solvents. The excitation laser used is 375 nm with a pulse width of less than 100 ps. **1-4AP** derivatives in chloroform were found to have lifetime significantly shorter than the excitation pulse width. The solution state fluorescence quantum yields were determined by using optically matched solutions. Quinine sulfate dissolved in 0.5 M H_2SO_4 ($\Phi_f = 0.546$)[1] is used as the standard for **1-4AP** derivatives. The solid state quantum yield of crystalline **1-4AP** was measured using an integrating sphere for which the accuracy was verified using tris(8-

hydroxyquinolinate)aluminium (Alq_3) as a standard and is determined to be 0.37 ± 0.04 (reported quantum yield $\Phi_f = 0.40$).[2] Radiative (k_r) and non-radiative (k_{nr}) decay rate constants can be calculated by using the equations 4 and 5.

$$\Phi = \frac{k_r}{k_r + k_{nr}} \quad (2)$$

$$\tau_f = \frac{1}{k_r + k_{nr}} \quad (3)$$

$$k_r = \frac{\Phi}{\tau_f} \quad (4)$$

$$k_{nr} = \frac{1}{\tau_f} - k_r \quad (5)$$

where Φ is the fluorescence quantum yield and τ_f is the fluorescence lifetime. In solution radiative (k_r) and non-radiative (k_{nr}) rate constants were calculated considering a lifetime of 100 ps (pulse duration of the excitation source), as **1-4AP** derivatives in chloroform were found to have lifetime significantly shorter than the excitation pulse width (~100 ps). In case of multi-exponential decay as in the case of crystalline **1-4AP**, the weighted average of the fluorescence lifetime values was used for estimation of rates of radiative and non-radiative processes which could be calculated using equation 6,[3]

$$\tau_f = \frac{\alpha_1\tau_1^2 + \alpha_2\tau_2^2 + \alpha_3\tau_3^2 + \ldots}{\alpha_1\tau_1 + \alpha_2\tau_2 + \alpha_3\tau_3 + \ldots} \quad (6)$$

where α = amplitude corresponding to the fluorescence lifetime (τ_f) decay.

Analysis of Chromaticity Index: Coordinates (x, y, z) for chromaticity are acquired by calculating the fractional component of the tristimulus values: x = X/(X+Y+Z), y = Y/(X+Y+Z), z = Z/(X+Y+Z). X, Y, Z are the CIE 1931 tristimulus values. By convention, chromicity coordinates (x, y) denote the two dimensional plot CIE 1931 colour space chromaticity diagram.

X-ray Crystallography: High-quality specimens of appropriate dimensions were selected for the X-ray diffraction experiments. Crystallographic data collected are presented in the supplementary information. Single crystals were mounted using oil (Infineum V8512) on a glass fibre. All measurements were made on a CCD area detector with graphite monochromated Mo Kα radiation. The data was collected using Bruker APEXII detector and processed using APEX2 from Bruker. All structures were solved by direct methods and expanded using Fourier techniques. The non-hydrogen atoms were refined anisotropically. Hydrogen atoms were included in idealized positions, but not refined. Their positions were constrained relative to their parent atom using the appropriate HFIX command in SHELXL-97. The full validation of CIFs and structure factors of **1-4AP** derivatives were performed using the CheckCIF utility and found to be free of major alert level. 3D structure visualization and the exploration of the crystal packing of **1-4AP** were carried out using Mercury 3.1.

Computational methods

Quantum Theory of Atoms in Molecules (QTAIM): The wave function for the derivatives **1-4AP** were obtained employing the geometries taken from the crystal structure using Gaussian set of codes at B3LYP/6-311++G** level.[4] Quantum theory of atoms in molecules (QTAIM) analysis helps to understand the description of interatomic interaction in the single crystal X-ray structure. A bond is defined along the bond line between two nuclei, called a bond path, along which electron density is concentrated. In a three dimensional space there are four types of critical points, corresponding to non-degenerate points: termed (3, -3), (3, -1), (3, +1) and (3, +3). The (3, -3) and (3, +3) types represent a maximum (which corresponds to a nuclear position) and a minimum, respectively. While (3, -1) and (3, +1) types represent saddle points called bond critical points and the ring critical points, respectively. There is also a second set of special gradient paths conjugated to the bond paths which starts at infinity but terminates at the bond critical point instead of being attracted to a nucleus.

Therefore, this bundle of paths does not belong to any atom and form a surface called the interatomic surface. The bond critical point (BCP) is a point along the bond path at the interatomic surface, where the shared electron density reaches a minimum. The physical characteristics of the BCPs [the electron density at BCP, $\rho(r_{\mathrm{BCP}})$, and its Laplacian, $\nabla^2\rho(r_{\mathrm{BCP}})$] reveal the approximate measure of the amount of electron density built up in the bonding region and as such could be taken as characteristic of the bond. When $\nabla^2\rho(r_{\mathrm{BCP}}) < 0$ and is large in magnitude, $\rho(r_{\mathrm{BCP}})$ is also large which means that there is a concentration of electronic charge in the internuclear region. This is also an indication of a sharing of electronic charge between both nuclei that defines the covalent (polar) bond. When $\nabla^2\rho(r_{\mathrm{BCP}}) < 0$ there is a depletion of electronic charge in the internuclear region. Using the AIM 2000 software package, the electron density was integrated over atomic basins according to the quantum theory of atoms in molecules using PROAIM, and thus the BCP data and the molecular graphs were obtained.

Hirshfeld Analysis: Important intermolecular interactions within the crystal structure of **1-4AP** were identified through Hirshfeld surface analysis using Crystal Explorer 3.0. The Hirshfeld surface is defined as a set of points in 3D space where the ratio of promolecule and procrystal electron densities is equal to 0.5. The exploration of intermolecular contacts is provided by mapping normalized contact distances (d_{norm}), which is a function of a closest distance from the point to the nuclei interior (d_{i}) and exterior (d_{e}) to the surface as well as on the van der Waals radii (r^{vdw}). 2D fingerprint which were generated by deriving from the Hirshfeld surface by plotting the fraction of points on the surface as the fuction of d_{i} and d_{e} which provide a visual summary of intermolecular contacts within the crystal.

Synthesis procedure and characterisation:

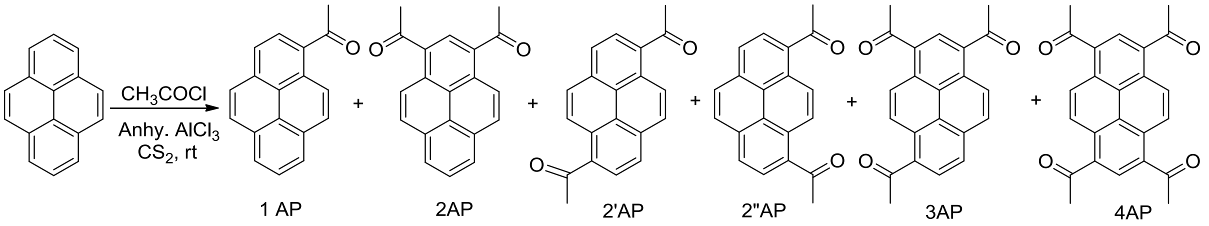

Scheme S1 Shows the synthesis of acetylpyrene (**1-4AP**) derivatives.

Preparation of acetylpyrene (1-4AP) derivatives:[5] Pyrene dissolved in CS_2 (yellow solution) was maintained at ambient temperature and subsequently anhydrous $AlCl_3$ was added. Acetyl chloride was then slowly syringed to the suspension. Subsequently, hydrogen chloride was liberated. After 3 hrs the mixture was added slowly to a vigorously stirred mixture of ice and concentrated HCl. The resulting suspension was filtered and vacuum dried and purified through column chromatography (silica gel) to give acetylpyrene (**1-4AP**) derivatives.

1AP (**yield= 5.1%**). M.p. 90.4°C. ^{1}H NMR [500 MHz, $C_2D_2Cl_4$, δ]: 9.09 (d, *J*= 9.35 Hz, 1H), 8.43 (d, *J* = 8.05 Hz, 1H), 8.33 (d, *J* = 2.9 Hz, 1H), 8.32 (d, *J* = 2.9 Hz, 1H), 8.29 (d, *J* = 9.4 Hz, 1H), 8.24 (d, *J* = 1.35 Hz, 1H), 8.22 (s, 1H), 8.13 (m, 2H), 2.96 (s, 3H). ^{13}C NMR [125 MHz, $C_2D_2Cl_4$, δ]: 202.57, 134.08, 131.96, 131.11, 130.47, 129.91, 129.86, 129.40, 127.37, 127.31, 126.72, 126.67, 126.34, 125.06, 124.97, 124.30, 124.26, 30.74. IR (KBr, cm^{-1}): 3041, 1675, 1249. Elemental analysis: calcd. value for $C_{18}H_{12}O$: 88.50% C, 4.95% H; found: 88.78% C, 4.88% H. HRMS (EI) *m/z* calculated for $C_{18}H_{12}O$ $[M]^+$: 244.0888, found: 244.0872.

2AP (**yield= 9.4%**). M.p. 179.0°C. ^{1}H NMR [500 MHz, DMSO (d_6), δ]: 8.87 (s, 1H), 8.78 (d, *J* = 9.30 Hz, 2H), 8.38 (d, *J* =7.65 Hz, 2H), 8.35 (d, *J* = 9.35 Hz, 2H), 8.13 (t, *J* = 7.60 Hz, 1H), 2.88 (s, 6H). ^{13}C NMR [125 MHz, DMSO (D_6), δ]: 201.94, 131.41, 131.21, 130.37, 129.87, 128.03, 127.43, 127.20, 124.39, 124.18, 123.19, 30.71. IR (KBr, cm^{-1}): 3048, 1681, 1249. Elemental analysis: calcd.

value for $C_{20}H_{14}O_2$: 83.90% C, 4.93% H; found: 84.07% C, 4.93% H. HRMS (EI) *m/z* calculated for $C_{20}H_{14}O_2$ $[M]^+$: 286.0994, found: 286.0991.

2’AP (**yield= 9.6%**) M.p. 205.7°C. ^{1}H NMR [500 MHz, DMSO (d_6), δ]: 8.86 (d, *J* = 9.35 Hz, 2H), 8.55 (d, *J* = 8.05 Hz, 2H), 8.35 (d, *J* = 8.05 Hz, 2H), 8.28 (d, *J* = 9.40 Hz, 2H), 2.83 (s, 6H). ^{13}C NMR [125 MHz, DMSO (D6), δ]: 202.20, 133.33, 132.31, 129.07, 128.20, 127.73, 126.39, 125.35, 123.73, 30.64. IR (KBr, cm-1): 3028, 1676, 1251. Elemental analysis: calcd. value for $C_{20}H_{14}O_2$: 83.90% C, 4.93% H; found: 83.96% C, 4.90 % H. HRMS (EI) *m/z* calculated for $C_{20}H_{14}O_2$ $[M]^+$: 286.0994, found: 286.0986.

2”AP (**yield= 37.5%**) M.p. 161.6°C. ^{1}H NMR [500 MHz, DMSO (d_6), δ]: 8.87 (s, 2H), 8.55 (d, *J* = 8.0 Hz, 2H), 8.37 (d, *J* = 8.0 Hz, 2H), 8.27 (s, 2H), 2.82 (s, 6H). ^{13}C NMR [125 MHz, DMSO (D_6), δ]: 202.02, 133.21, 132.81, 129.14, 127.83, 127.43, 126.40, 125.78, 123.75, 30.58. IR (KBr, cm^{-1}) 3000, 1659, 1231. Elemental analysis: calcd. value for $C_{20}H_{14}O_2$: 83.90% C, 4.93% H; found: 83.96% C, 4.89 % H. HRMS (EI) *m/z* calculated for $C_{20}H_{14}O_2$ $[M]^+$: 286.0994, found: 286.0981.

3AP (**yield= 18.9%**) M.p. 178.8°C. ^{1}H NMR [500 MHz, $CDCl_3$, δ]:9.13 (d, *J* = 9.5 Hz, 1H), 9.02 (d, *J* = 9.0 Hz, 1H), 9.0 (d, *J* = 9.5 Hz, 1H), 8.70 (s, 1H), 8.47 (d, *J* = 8.0 Hz, 1H), 8.34 (d, *J* = 8.0 Hz, 1H), 8.29 (d, *J* = 9.5 Hz, 1H), 2.97 (s, 6H), 2.95 (s, 3H). ^{13}C NMR [125 MHz, $CDCl_3$, δ]: 201.72, 201.19, 201.15, 133.87,132.46, 131.96, 131.91, 131.18, 130.66, 130.32, 128.51, 128.09, 127.66, 127.31, 126.17, 126.08, 126.04, 124.67, 123.90, 30.52, 30.51, 30.46. IR (KBr, cm^{-1}): 3020, 1664, 1255. Elemental analysis: calcd. value for $C_{22}H_{16}O_3$: 80.47% C, 4.91% H; found: 80.63% C, 4.87% H. HRMS (EI) *m/z* calculated for $C_{22}H_{16}O_3$ $[M]^+$: 328.1099, found: 328.1086.

4AP (**yield= 4.6%**) M.p. 295.6°C. ^{1}H NMR [500 MHz, $C_2D_2Cl_4$, δ]: 9.04 (s, 4H), 8.70 (s, 2H), 2.99 (s, 12H). ^{13}C NMR [125 MHz, $CDCl_3$, δ]: 201.80, 134.01, 133.96, 130.47, 128.21, 127.25, 125.25, 30.97. IR (KBr, cm^{-1}): 3004, 1685, 1270. Elemental analysis: calcd. value for $C_{24}H_{18}O_4$: 77.82% C, 4.90% H; found: 77.61% C, 4.85% H. HRMS (EI) *m/z* calculated for $C_{24}H_{18}O_4$ $[M]^+$: 370.1205, found: 370.1211.

Table S1. Shows crystallographic data and refinement parameters for crystalline **1-4AP** derivatives.

	1AP	**2AP**	**2’AP**	**2”AP**	**3AP**	**4AP**
formula	$C_{18}H_{12}O$	$C_{20}H_{14}O_2$	$C_{20}H_{14}O_2$	$C_{20}H_{14}O_2$	$C_{22}H_{16}O_3$	$C_{24}H_{18}O_4$
formula wt	244.28	286.31	286.31	286.31	328.35	370.38
colour, shape	Pale Yellow	Yellow	Yellow	Yellow	Yellow	Orange
dimens, mm	0.20x0.15x0.10	0.20x0.15x0.10	0.25x0.20x0.15	0.20x0.15 x0.10	0.20x0.15x0.10	0.20x0.10x0.10
crystal system	Monoclinic	Orthorhombic	Monoclinic	Monoclinic	Monoclinic	Monoclinic
space group, Z	Cc	Pnma	P2(1)/n	P2(1)/c	P2(1)/c	C_2
a, Å	34.4472	7.3519	9.243	8.1941	11.0402	20.1864
b, Å	7.3598	16.6654	7.463	23.0417	20.0564	39.6060
c, Å	9.8621	11.3344	10.095	7.4020	7.2682	7.0261
α, deg	90.00	90.00	90.000	90.00	90	90.00
β, deg	98.492	90.00	98.880	93.824	96.682	109.988
γ, deg	90.00	90.00	90.000	90.00	90	90.00
V, Å^3	2472.87	1388.72	688.0	1394.43	1598.44	5279.0
temp, K	296	296	296	296	296	293
*d*calcd, g/cm^{-3}	1.312	1.369	1.382	1.364	1.364	1.398
no. of reflections collected	9183	5744	4832	10022	12353	15979
no. of unique reflections	3756	1269	1200	2408	2825	8235
$2\theta_{max}$, deg	50	50	50	50	50	50
no. of parameters	343	106	128	201	226	1023
$R1$, $wR2$ ($I > 2\sigma(I)$)	0.0418, 0.1111	0.0427, 0.1126	0.0416, 0.1148	0.0764, 0.1157	0.0612, 0.1756	0.0893, 0.2275
$R1$, $wR2$ (all data)	0.0489, 0.1268	0.0601, 0.1277	0.0562, 0.1229	0.1201, 0.1314	0.1276, 0.2316	0.1412, 0.2631
goodness of fit	1.053	1.036	1.069	1.068	1.061	1.069
CCDC number	CCDC 984436	CCDC 984437	CCDC 984438	CCDC 984439	CCDC 984440	CCDC 984441

Table S2. Shows melting temperature (T_m) and change in enthalpy (ΔH**)** values for crystalline **1-4AP** derivatives.

	^aT_m (°C)	^{b}ΔH (kJ/mole)
1AP	90.4	25.24
2”AP	161.7	29.45
2AP	179.0	32.41
3AP	178.8	36.86
2’AP	205.7	42.00
4AP	295.6	47.96

[a] Melting temperature [b] Change in enthalpy during melting

Table S3. Shows intramolecular (CH_3) H···H (aryl) (Å) distance (*d*) in crystalline **1-4AP** derivatives that is less than the sum of van der Waals radii of two hydrogen atoms (2.4 Å).

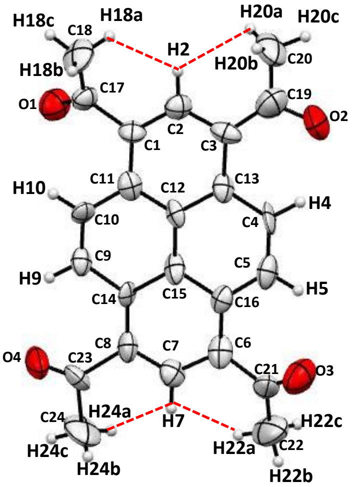

	Interaction	*d*, (Å)
1AP	H18a···H2	2.183
2AP	H18a···H2	2.098
	H20a···H2	2.098
2’AP	H18a···H2	2.350
	H22a···H7	2.350
2”AP	H18a···H2	2.315
	H24a···H7	2.356
3AP	H18a···H2	2.186
	H20a···H2	2.146
	H22a···H7	2.144
4AP	H18a···H2	2.078
	H20a···H2	2.186
	H22a···H7	2.055
	H24a···H7	2.139

Table S4. Shows calculated topological properties of the electron density for the intra- and intermolecular interaction in **2**, **3** and **4AP** derivatives.

Description	Interaction	[a]*d*, (Å)	[b]$\rho_b(r)$, e Å^{-3}	[c]$\nabla^2\rho_b(r)$, e Å^{-5}
2AP	H18c···H’18c	2.230	0.036	0.520
	O1···H10	2.325	0.093	1.354
	O2···H4	2.335	0.093	1.354
	O’1···H’10	2.335	0.093	1.356
	O’2···H’4	2.335	0.093	1.355
3AP	H20c···H’8	2.246	0.041	0.471
	H20c···H’9	2.579	0.019	0.249
	O1···H10	2.185	0.127	1.892
	O2···H4	2.199	0.123	1.838
	O3···H5	2.298	0.101	1.474
	O’2···H’4	2.199	0.123	1.836
	O2···H’9	3.242	0.013	0.182
	O’3···H’5	2.299	0.101	1.473
	O’1···H’10	2.185	0.127	1.892
4AP	H’18c···H”22c	2.239	0.040	0.514
	H’4···H18a	2.394	0.034	0.450
	H’5···H18c	2.577	0.023	0.300
	O2···H4	2.186	0.128	1.897
	O4···H9	2.210	0.121	1.785
	O1···H10	2.322	0.096	1.411
	O3···H5	2.354	0.091	1.314
	O’1···H”22c	2.490	0.062	0.708
	O”3···H’18c	2.490	0.062	0.708
	O’3···H’5	2.186	0.127	1.897
	O’1···H’10	2.210	0.121	1.786
	O’4···H’9	2.322	0.095	1.412
	O’2···H’4	2.354	0.091	1.313
	O”4···H9	2.354	0.091	1.312
	O”3···H”5	2.210	0.120	1.785
	O’2···H20b	3.309	0.013	0.175
	O”1···H”10	2.186	0.127	1.898
	O”2···H”4	2.322	0.096	1.411

[a]*d*=distance, [b]$\rho_b(r)$=electron density at the BCP and [c]$\nabla^2\rho_b(r)$= Laplacian of the electron density at the BCP

Table S5. Shows the percentage of intermolecular contacts of a molecule in crystalline **1-4AP** derivatives.

Interaction	**1AP**	**2AP**	**2’AP**	**2”AP**	**3AP**	**4AP**
H···H %	38.8	42.3	40.8	42.7	45.8	45.3
C···H %	46.9	26.4	35.9	27.0	13.2	7.4
O···H %	11.3	19.0	15.0	18.5	21.4	25.8
C···C %	2.4	10.3	3	9.9	14.8	16.1
C···O %	0.5	1.9	5.3	1.8	4.2	4.7

[a]total percentage of intermolecular contacts ca. 99.9% (**1AP**), 99.9% (**2AP**), 100% (**2’AP)**, 99.9% (**2”AP)**, 99.4% (**3AP)**, 99.3% (**4AP)**.

Table S6. Shows interplanar angle between nearest pyrene molecules in crystalline **1-4AP** derivatives.

	Angle, deg
1AP	48.4, 50.5, 51.1
2AP	11.1
2’AP	30.2
2’’AP	14.5
3AP	7.2
4AP	0, 3.9, 5.9

Table S7. Shows the photophysical properties of **1-4AP** derivatives.

	[a]λ_{abs} (nm)	[a]λ_{f} (nm)	[a]Φ_{f}	[a]τ_{f} (ns) [Amplitude] (%)	[a]k_{r}	[a]k_{nr}	[b]λ_{abs} (nm)	[b]λ_{f} (nm)	[b]τ_{f} (ns) [Amplitude] (%)	[b]Φ_{f}	[b]k_{r}	[b]k_{nr}
P	337	393	0.75[6]	150.1 [100][7]	5 x 10^{6}	1.6 x 10^{6}	386	472	22.97 [100]	0.67[8]	2.9 x 10^{7}	1.4 x 10^{7}
1AP	359	412	0.004	1.39 [93] 0.98 [7]	2.9 x 10^{6}	7.3 x 10^{8}	414	518	574.6 [15.7], 54.43 [68.5], 2873 [15.8]	0.006	2.6 x 10^{3}	4.3 x 10^{2}
2AP	373	426	0.008[c]	1.39 [93] 0.65 [7]	5.8 x 10^{6}	7.3 x 10^{8}	426	602	9.68 [46.5], 23.19 [30.9], 2.94 [22.6]	0.325	1.9 x 10^{7}	4.0 x 10^{7}
		510		0.7[3] 1.35 [96] 3.0 [1]	-	-						
2’AP	369	420	0.002[c]	1.3 [80] 1.62 [20]	1.5 x 10^{6}	7.3 x 10^{8}	430	567	3.95 [38.6], 19.55 [39.2], 1.07 [22.2]	0.030	1.8 x 10^{6}	5.0 x 10^{7}
		530		0.8 [1] 1.36 [98] 4.22 [1]	-	-						
2”AP	375	413	0.008[c]	1.4 [97] 0.6 [3]	5.8 x 10^{6}	7.2 x 10^{8}	441	631	3.47 [34.9], 11.57 [65.1]	0.063	6.0 x 10^{6}	8.0 x 10^{7}
		535		0.8 [1] 1.4 [98] 4.9 [1]	-	-						
3AP	388	431	0.003[c]	1.2	2.5 x 10^{6}	8.3 x 10^{8}	471	645	22.48 [8.4], 4.57 [91.6]	0.277	2.7 x 10^{7}	7.0 x 10^{7}
		550		4.1 [67] 1.5 [33]	-	-						
4AP	407	435	0.002[c]	0.98	2.0 x 10^{6}	1.0 x 10^{9}	486	646	1.17 [10.3], 2.78 [46.9], 6.11 [63.4]	0.071	1.4 x 10^{7}	1.8 x 10^{8}
		535		0.85 [55] 3.8 [45]	-	-						

[a]chloroform solution; [b]crystalline state; abs – absorption; f – fluorescence; [c]overall quantum yield. Observed increase in the rate of radiative decay for crystalline **2**, **2’** and **2’’AP** when compared to **2**, **2’** and **2’’AP** in solution is indicative of the formation of ‘J’ type aggregate.

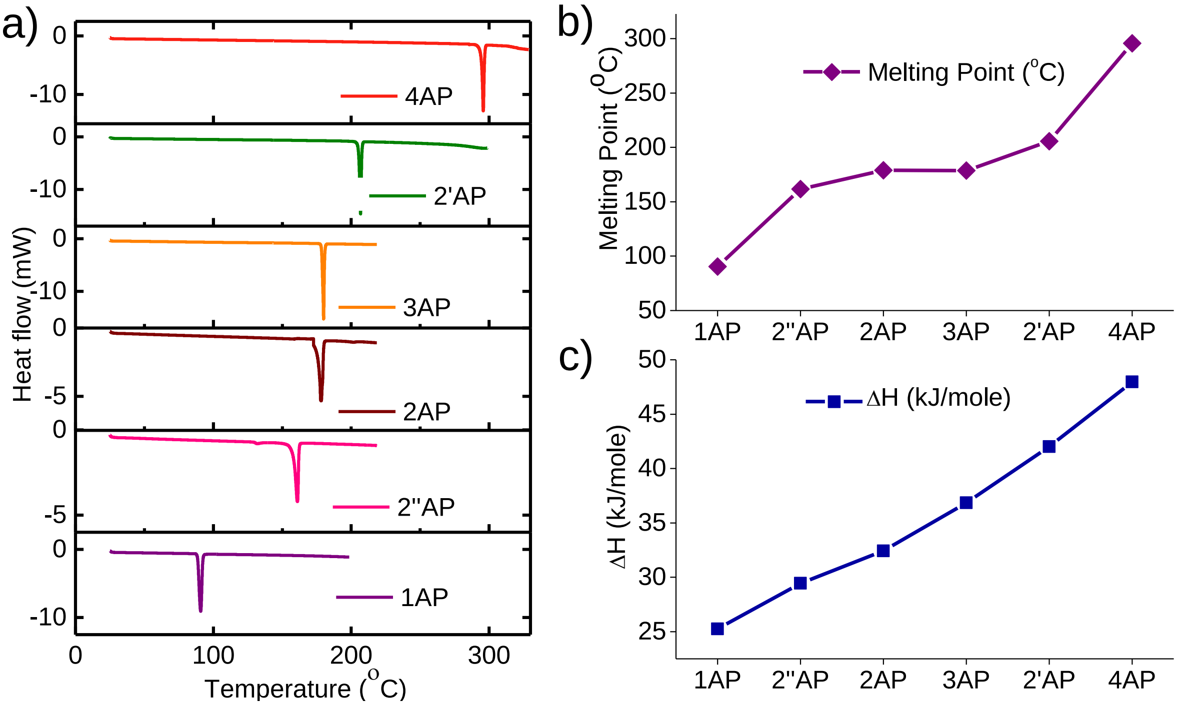

Fig. S1 Shows a) DSC melting temperature (T_m); b) near-linear increment in the melting temperature (T_m) and c) linear increment in the ΔH values of crystalline **1-4AP** derivatives.

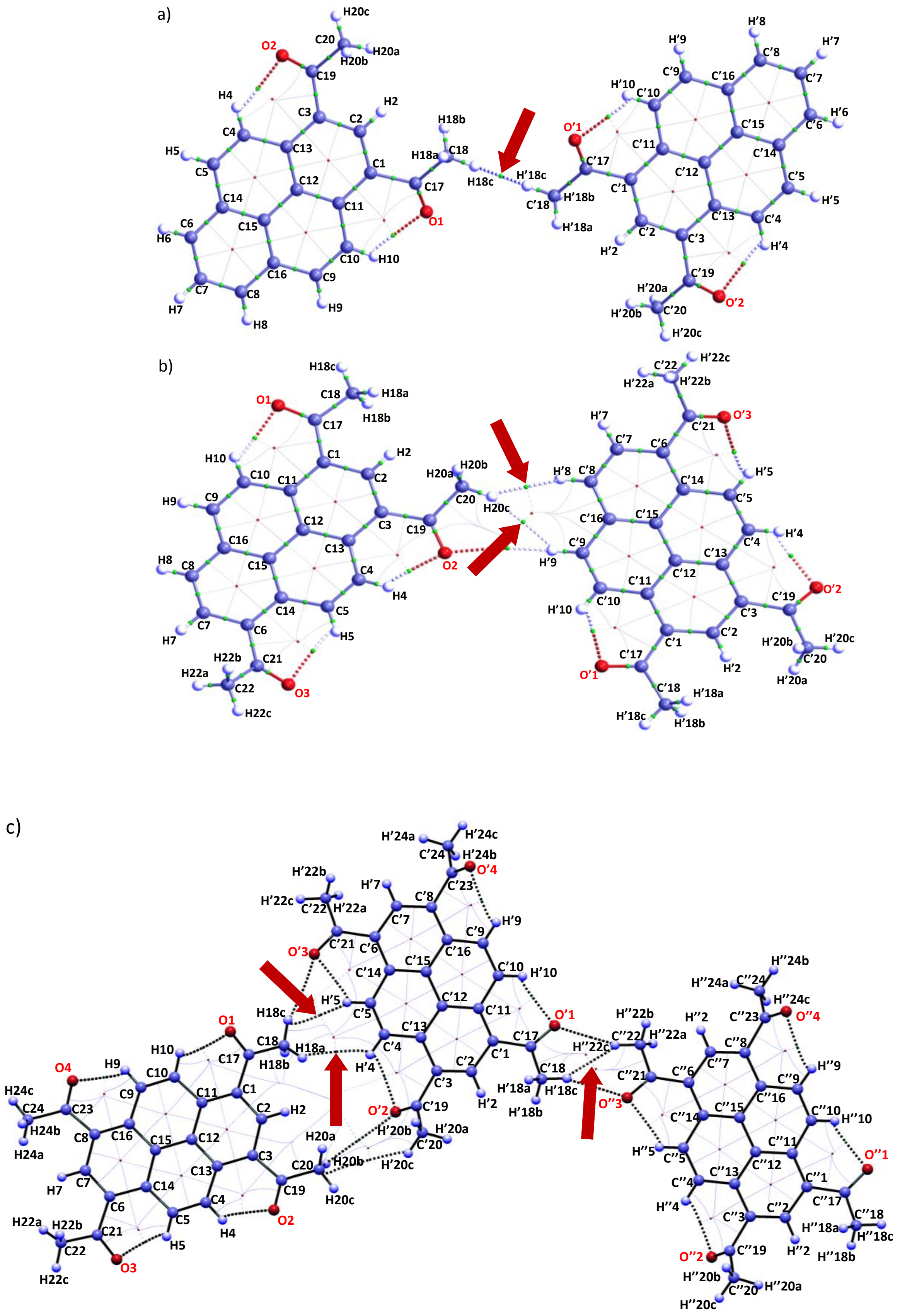

Fig. S2 Shows QTAIM electron density map of a) **2AP**; b) **3AP** and c) **4AP**, arrows indicate the existence of intermolecular C–H···H–C contacts.

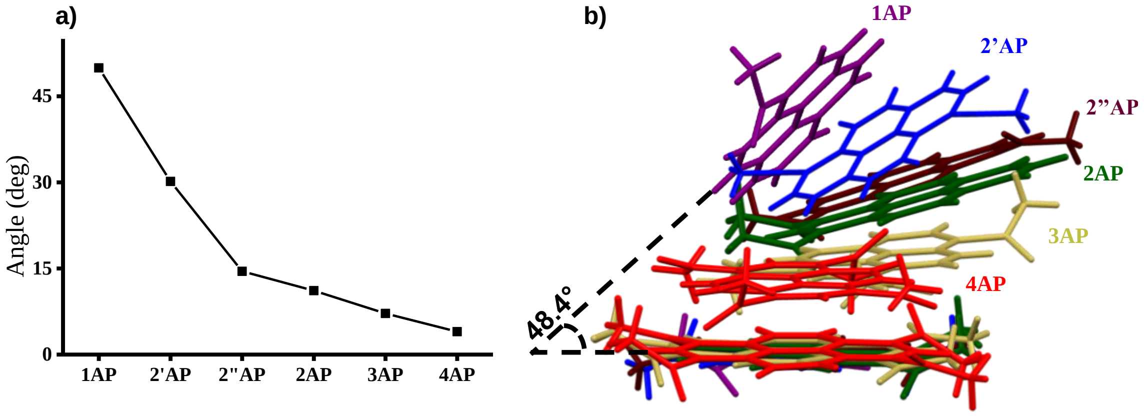

Fig. S3 Shows (a) the gradual decrease in the interplanar angle between the nearest molecules; (b) the decreasing angle and the consequent increase in stacking of the pyrene units in the crystalline **1-4AP** derivatives.

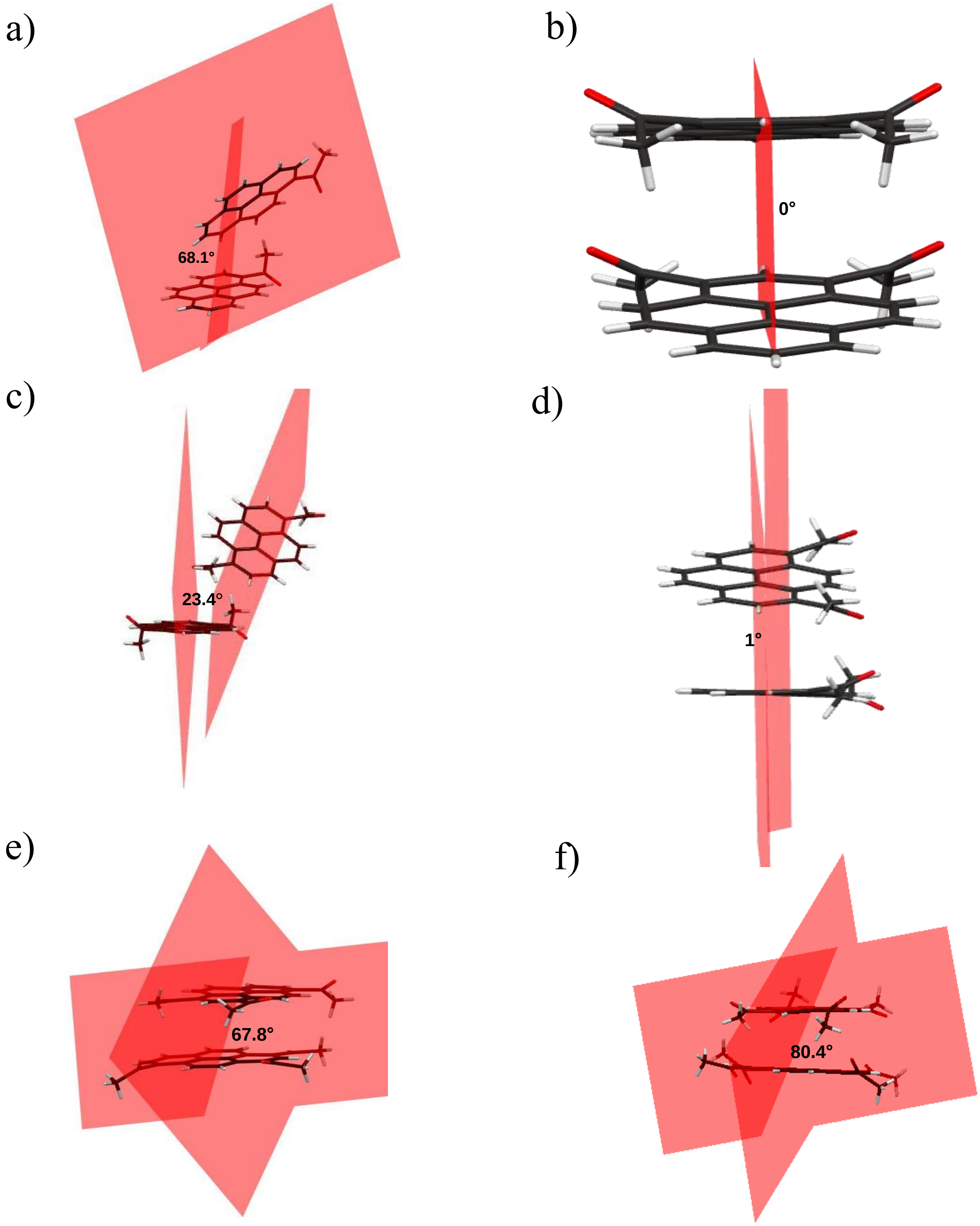

Fig. S4 Shows the torsional angle between adjacent pyrene units in crystal packing of a) **1AP**; b) **2AP**; c) **2’AP**; d) **2”AP**; e) **3AP** and f) **4AP**.

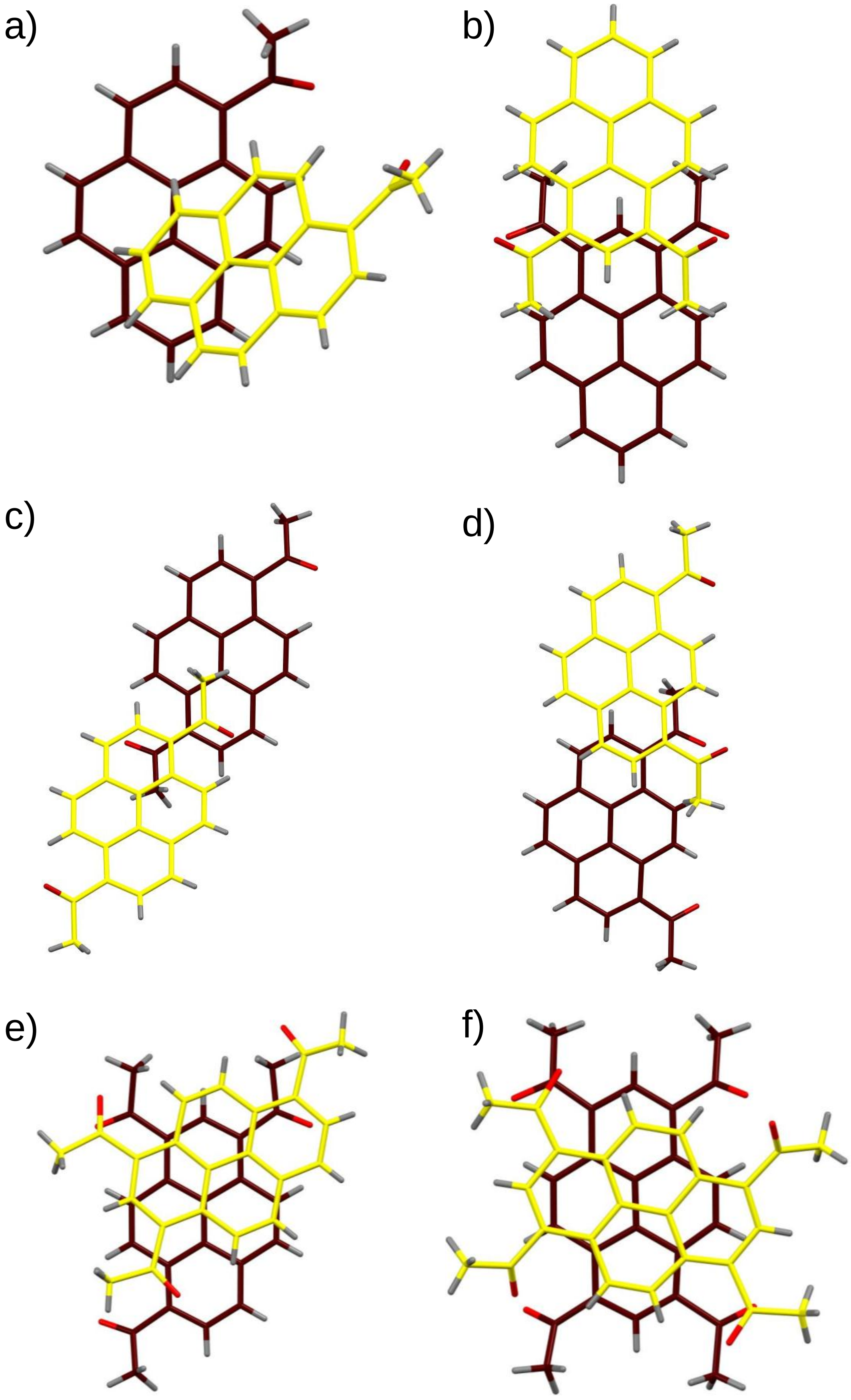

Fig. S5 Shows the aerial overlap between adjacent pyrene units in close packing of a) **1AP**; b) **2AP**; c) **2’AP**; d) **2”AP**; e) **3AP** and f) **4AP**.

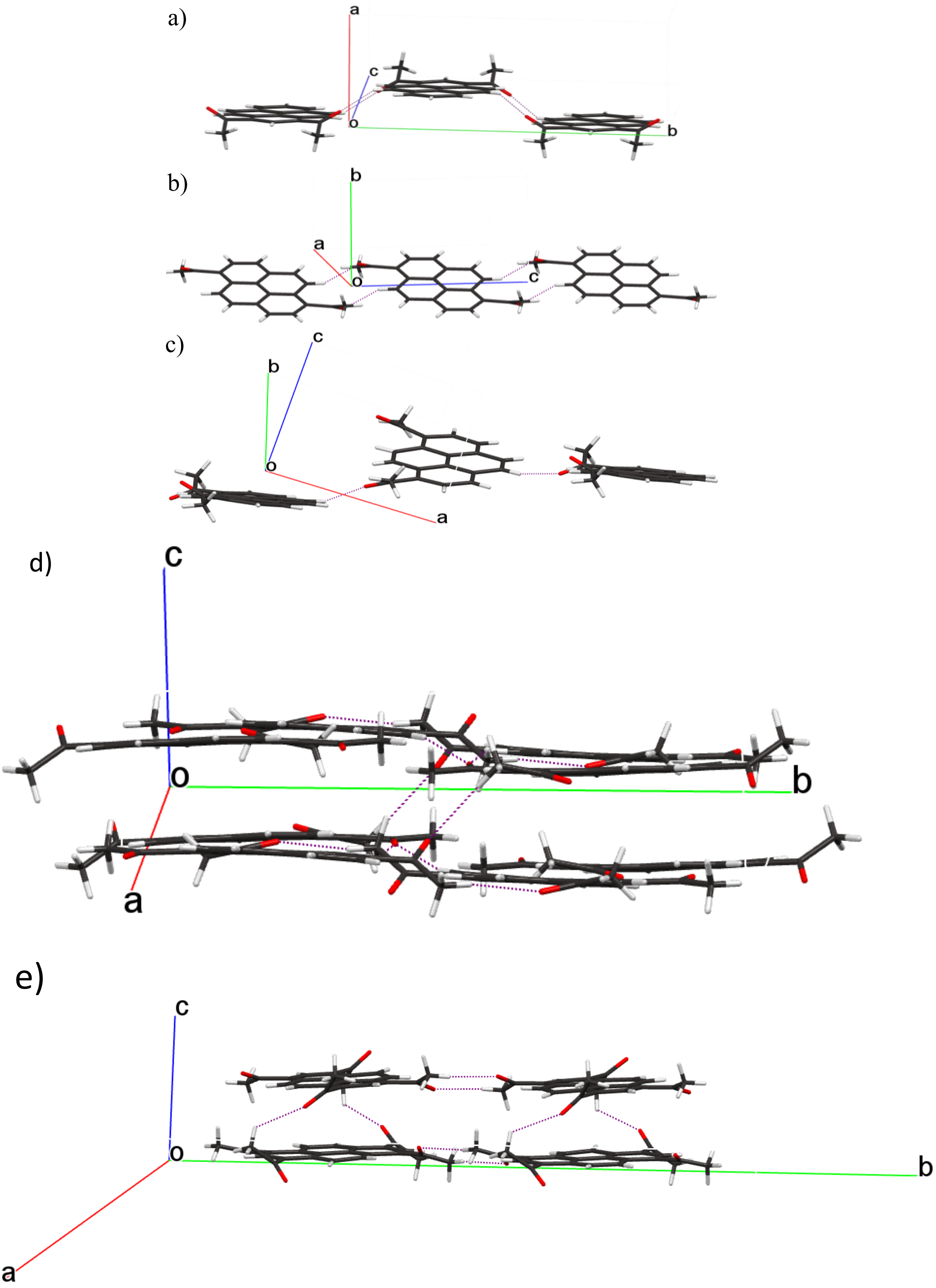

Fig. S6 Shows the C–H···O interactions in the crystal packing of a) **2AP**; b) **2’AP**; c) **2”AP**; d) **3AP** and e) **4AP**.

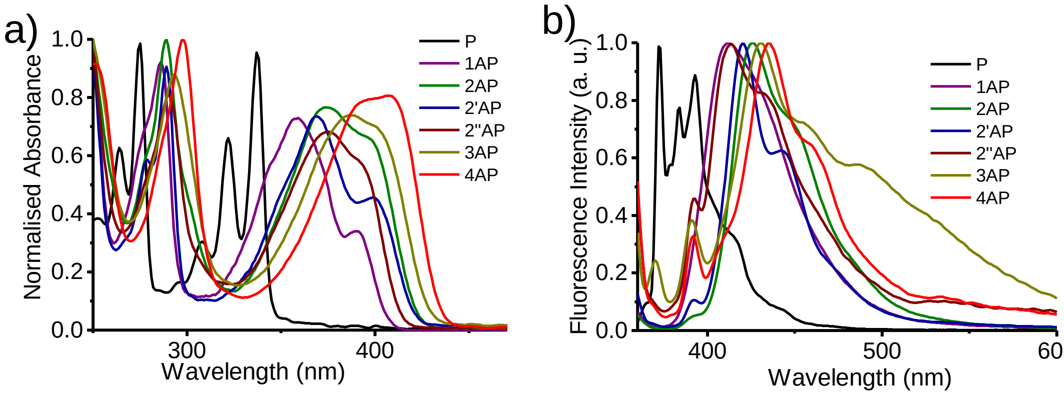

Fig. S7 Shows the normalised (a) absorption and (b) fluorescence spectra of **1-4AP** (0.1-1 μM) derivatives in $CHCl_3$.

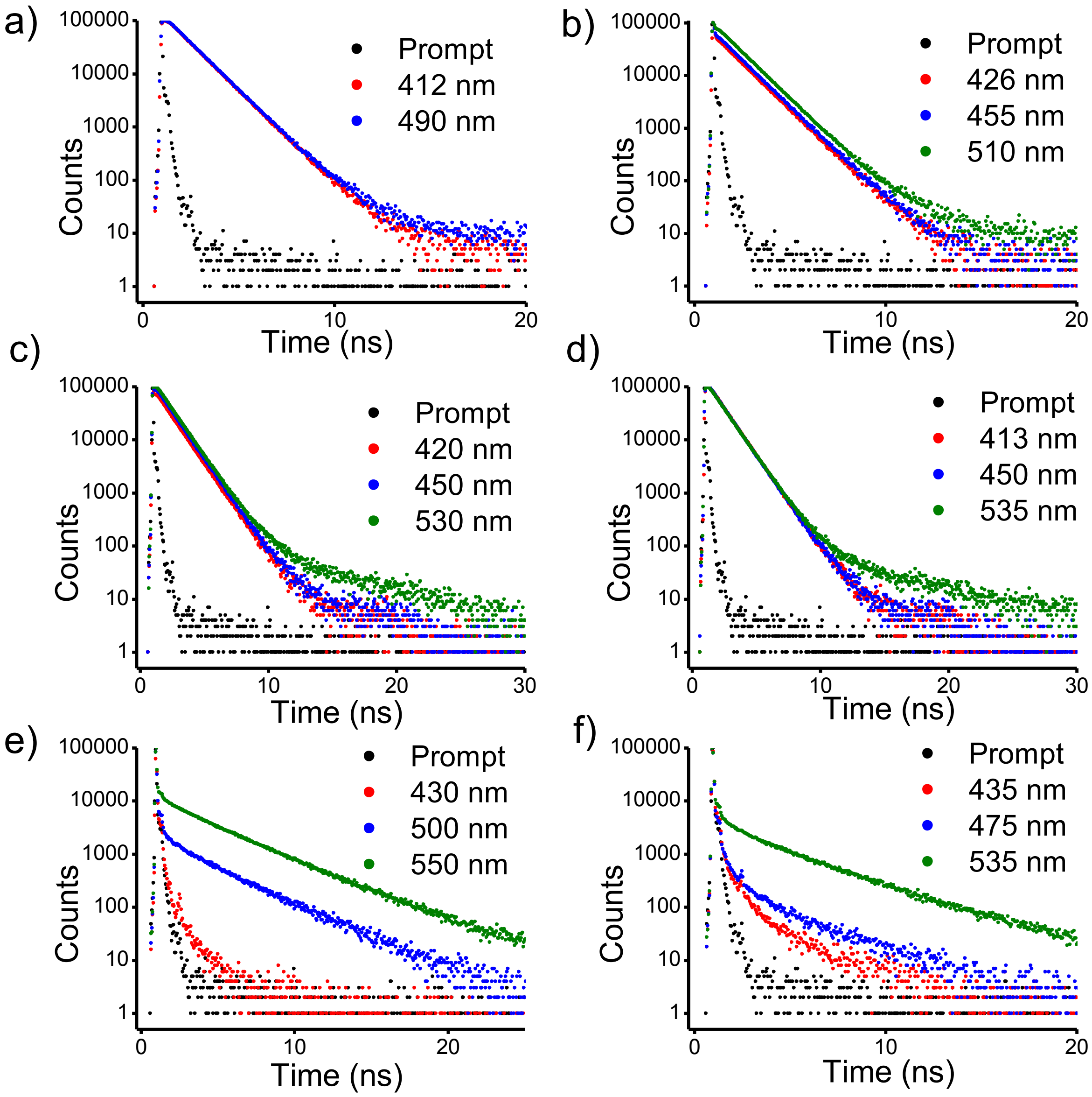

Fig. S8 Shows fluorescence decay profile of a) **1AP**; b) **2AP**; c) **2'AP**; d) **2"AP**; e) **3AP** and f) **4AP** in chloroform solution on exciting at 375 nm and collected at different wavelengths.

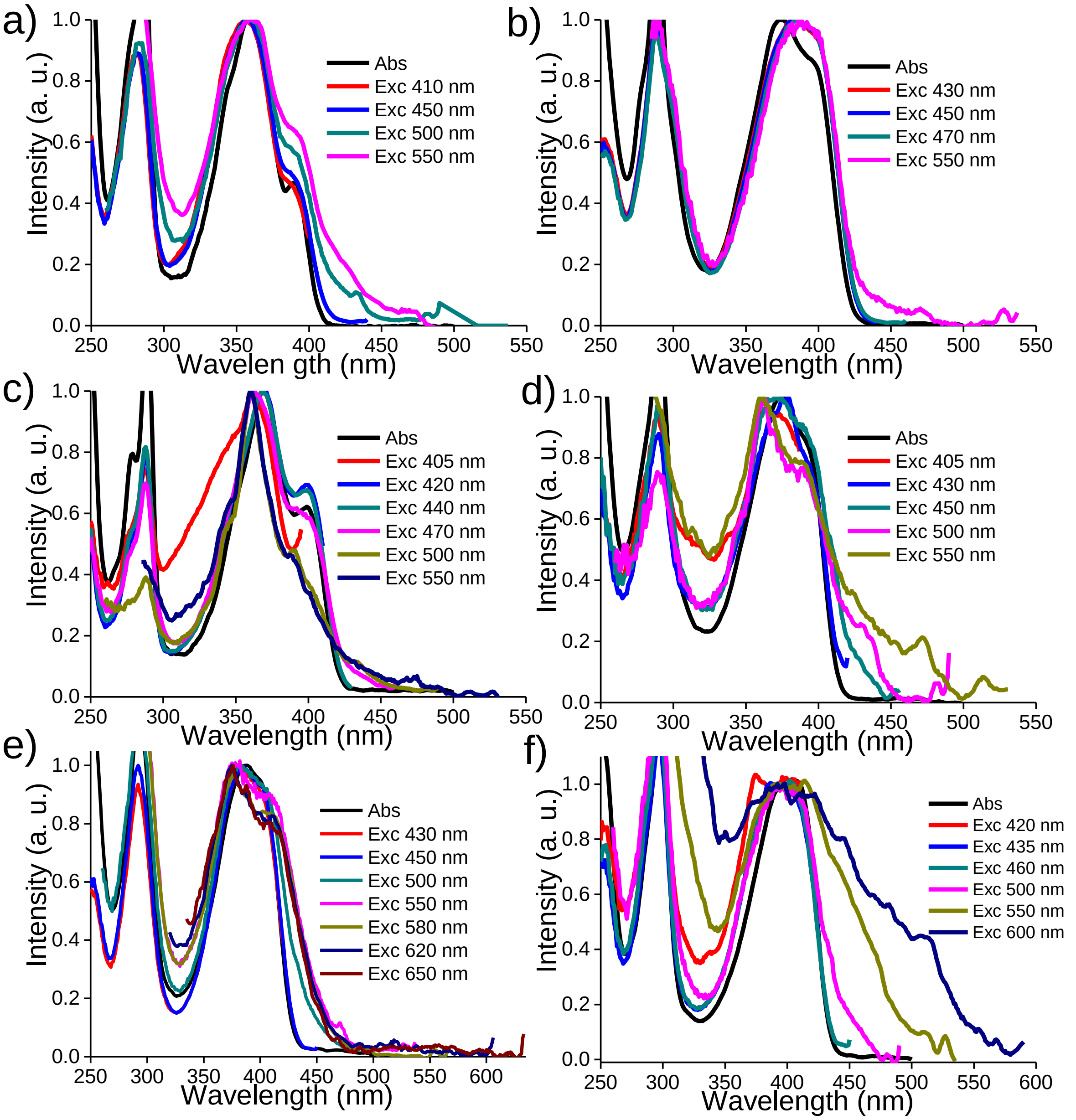

Fig. S9 Shows the fluorescence excitation spectra of a) **1AP**; b) **2AP**; c) **2’AP**; d) **2”AP**; e) **3AP** and f) **4AP** in $CHCl_3$ as compared to absorption spectrum.

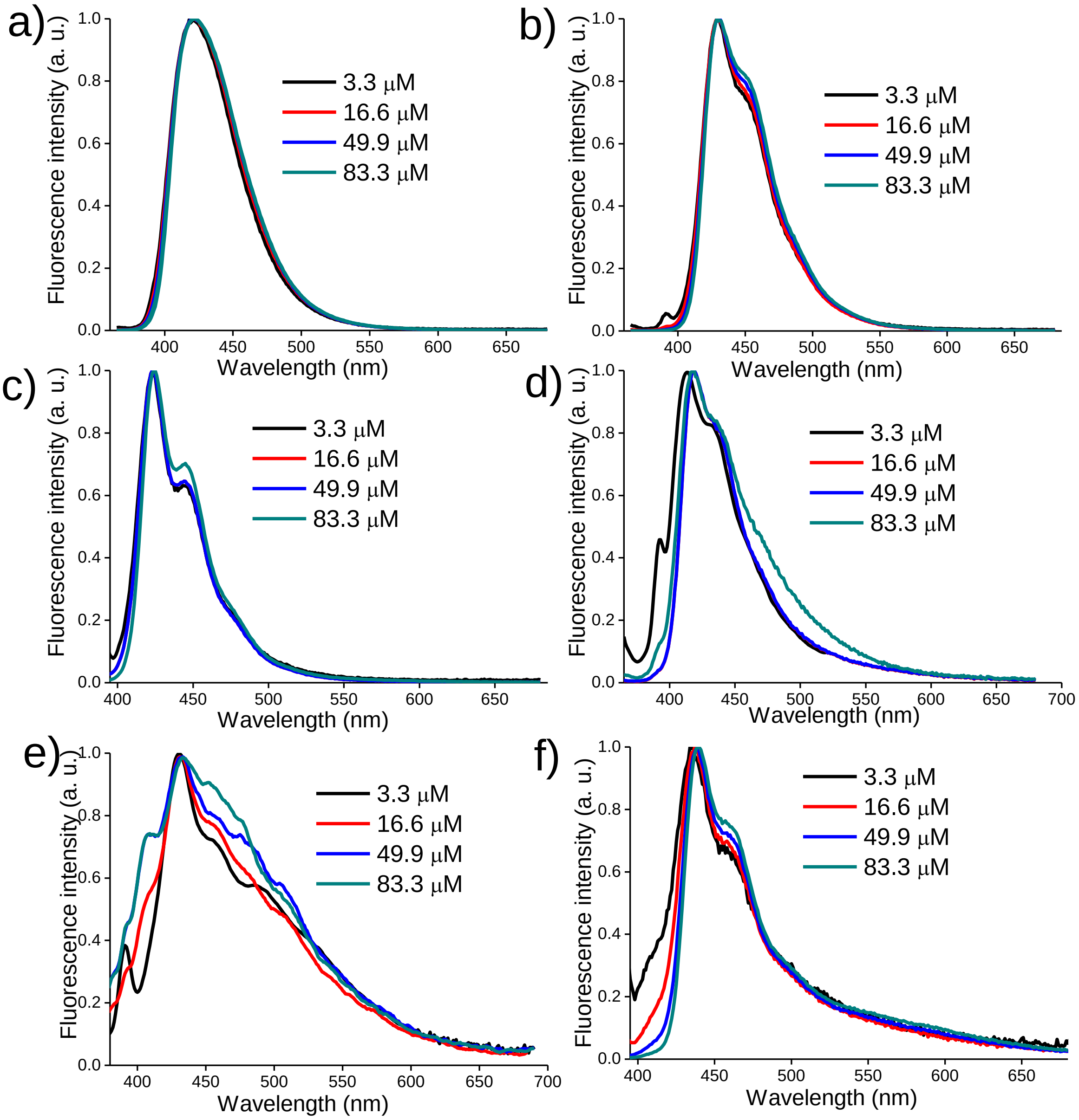

Fig. S10 Concentration dependent emission spectra of a) **1AP**; b) **2AP**; c) **2’AP**; d) **2”AP**; e) **3AP** and f) **4AP** in chloroform solution on exciting at 350 nm.

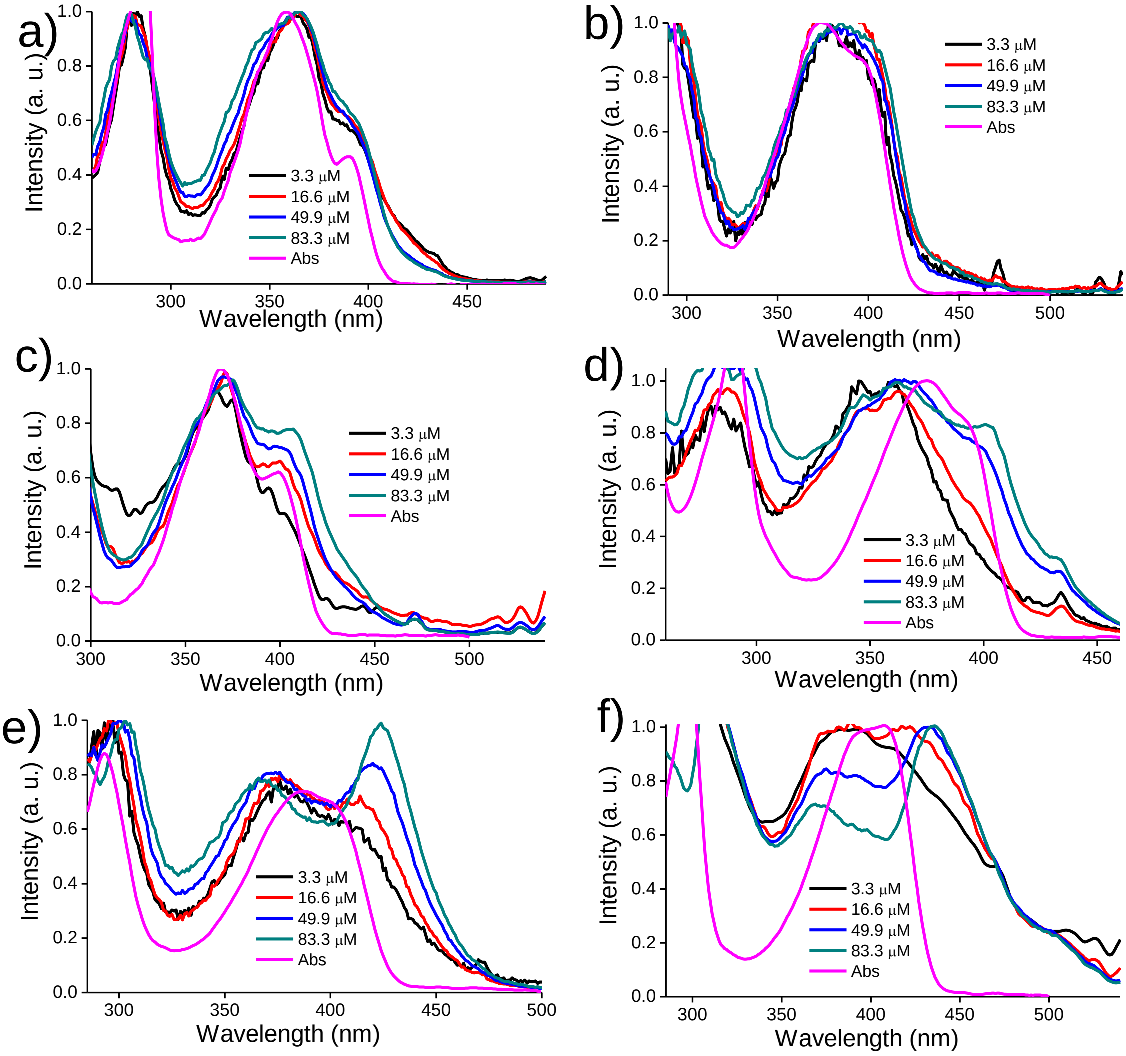

Fig. S11 Concentration dependent excitation spectra of a) **1AP**; b) **2AP**; c) **2’AP**; d) **2”AP**; e) **3AP** and f) **4AP** in chloroform solution while monitoring at 500 nm (for **1AP** and **2”AP)** and 550 nm (for **2AP**, **2’AP**, **3AP** and **4AP)**.

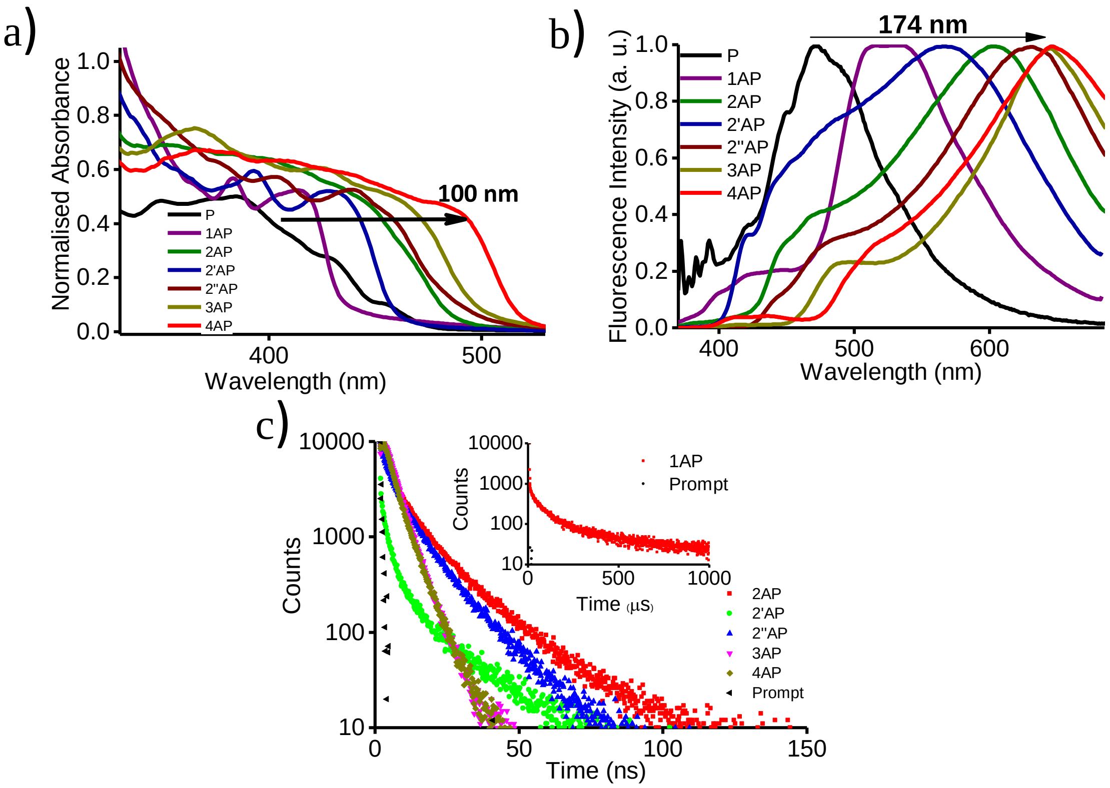

Fig. S12 Shows the normalised (a) absorption and (b) fluorescence emission spectra of crystalline **1-4AP** derivatives; excitation wavelength is 350 nm and (c) fluorescence decay profile of crystalline **2-4AP** derivatives and the corresponding inset shows fluorescence decay profile of crystalline **1AP**, excitation wavelength is 375 nm and emission monitored at 518 nm (**1AP**); 602 nm (**2AP**); 567 nm (**2'AP**); 631 nm(**2"AP**); 645 nm (**3AP**) and 646 nm (**4AP**).

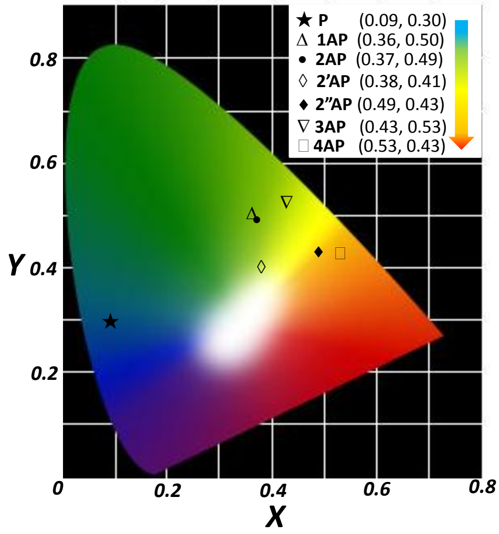

Fig. S13 Shows CIE colour diagram of fluorescence emission for crystalline **1-4AP** derivatives.

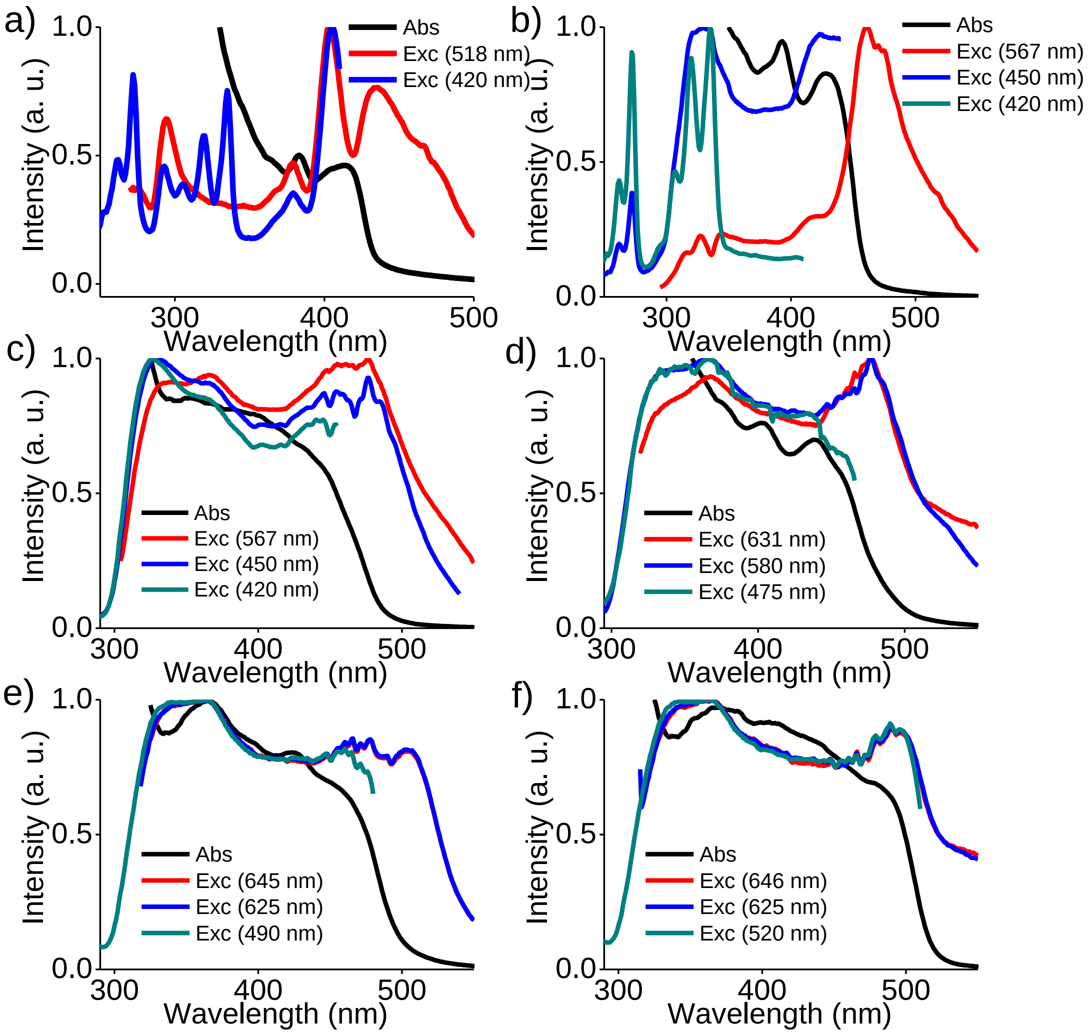

Fig. S14 Shows fluorescence excitation spectra of crystalline a) **1AP**; b) **2AP**; c) **2’AP**; d) **2”AP**; e) **3AP** and f) **4AP** as compared to absorption spectra. Absorption spectra of crystalline **1-4AP** derivative are reproduced from **Fig. S12a** for comparison with excitation spectra. Emission maxima, where the excitation spectra are monitored, are indicated in the bracket.

Reference

1. D. F. Eaton, *Pure Appl. Chem.*, 1988, **60**, 1107-1114.
2. M. Cölle, J. Gmeiner, W. Milius, H. Hillebrecht and W. Brütting, *Adv. Funct. Mater.*, 2003, **13**, 108-112.
3. J. R. Lakowicz, in *3rd ed.*, Springer, New York, 2006.
4. M. J. Frisch, G. W. Trucks, H. B. Schlegel, G. E. Scuseria, M. A. Rob, J. R. Cheeseman, J. A. Montgomery Jr., T. K. Vreven, K. N., J. C. Burant, J. M. Millam, S. S. Iyengar, J. Tomasi, V. Barone, B. Mennucci, M. Cossi, G. Scalmani, N. Rega, G. A. Petersson, H. Nakatsuji, M. Hada, M. Ehara, K. Toyota, R. Fukuda, J. Hasegawa, M. Ishida, Y. Nakajima, O. Honda, H. Kitao, M. Nakai, X. Klene, J. E. Li, H. P. Knox, J. B. Hratchian, T. Cross, V. Bakken, C. Adamo, J. Jaramillo, R. Gomperts, R. E. Stratmann, O. Yazyev, A. J. Austin, R. Cammi, C. Pomelli, J. W. Ochterski, P. Y. Ayala, K. Morokuma, G. A. Voth, P. Salvador, J. J. Dannenberg, V. G. Zakrzewski, S. Dapprich, A. D. Daniels, M. C. Strain, O. Farkas, D. K. Malick, A. D. Rabuck, K. Raghavachari, J. B. Foresman, J. V. Ortiz, Q. Cui, A. G. Baboul, S. Clifford, J. Cioslowski, B. B. Stefanov, G. Liu, A. Liashenko, P. Piskorz, I. Komaromi, R. L. Martin, D. J. Fox, T. Keith, M. A. Al-Laham, C. Y. Peng, A. Nanayakkara, M. Challacombe,

P. M. W. Gill, B. Johnson, W. Chen, M. W. Wong, C. Gonzalez and J. A. Pople, (Gaussian, Inc., Wallingford, CT, 2003).

5. R. G. Harvey, J. Pataki and H. Lee, *Org. Prep. Proced. Int.*, 1984, **16**, 144-148.
6. R. Katoh, S. Sinha, S. Murata and M. Tachiya, *J. Photochem. Photobiol. A: Chem.*, 2001, **145**, 23-34.
7. J. Kollár, P. Hrdlovič and Š. Chmela, *J. Photochem. Photobiol. A: Chem.*, 2010, **214**, 33-39.
8. R. Katoh, K. Suzuki, A. Furube, M. Kotani and K. Tokumaru, *J. Phys. Chem. C*, 2009, **113**, 2961-2965.